

Dynamic weakening of ring faults and catastrophic caldera collapse

Raehee Han*, Jong-Sun Kim, Chang-Min Kim, Takehiro Hirose, Jong Ok Jeong,
Gi Young Jeong

*E-mail: raeheehan@gnu.ac.kr

This file includes:

Methods
Figs DR1 to DR3
Tables DR1 to DR4

Methods

M1. Measurement of slip zone temperature

We used a high-resolution infrared thermal-imaging camera (Thermo Tracer TH9260) to measure the slip zone temperature during the high-velocity friction tests (e.g., Lee et al., 2017). We used a sampling frequency of 30Hz (or 30 frames per second). The resolution and the accuracy of temperature measurement were $90 \times 90 \mu\text{m}^2$ per pixel and $\pm 2^\circ\text{C}$ or $\pm 2\%$, respectively. For temperature determination, we used the emissivity values of 0.76 and 1.0 (Ramsey et al., 2012) as the end-members.

M2. Determination of the melting point of the rock (T_m)

T_m is defined as the temperature at the boundaries of a melt layer. The temperature recorded was the measurement made just before the onset of the final deceleration of slip in each experiment. In each specimen, the locations of the melt boundaries were inferred from the thickness (w) of the experimental PST. The measured temperature ranged from 966 to 1175 $^\circ\text{C}$, depending on the emissivity of the melt layer (0.76–1.0). We took 1071 $^\circ\text{C}$, the average of the temperature range, as T_m .

M3. Measurement of clast fraction (ϕ)

The experimental and natural PSTs were observed with an electron microscope, with backscattered electron images being taken over the entire area of the specimens. The images, at magnifications of 100–140×, were merged into a single image. By adjusting the contrast and making additional examinations of very fine clasts, a binary image showing the clast distribution was constructed (inset images in Fig. 3B and C). The areas of both the whole melt layer and the clasts were measured in terms of the number of pixels by using imaging software (NIS-Elements, Nikon). From this information, the ratio of the area of clasts to that of the melt layer was calculated. Pixels that were smaller than $0.568 \mu\text{m} \times 0.568 \mu\text{m}$ were not counted because of the applicable analytical limit.

M4. Estimation of V for the natural pseudotachylyte

The steady-state temperature distribution for a given product of steady-state shear stress (τ_{ss}) and slip rate (V) is (15):

$$T(z) = T_m - T_c \log \left(\frac{\cosh^2 \left(\frac{2z\tau_{ss}}{\eta_c W} \sqrt{\frac{V^2}{W^2} + 1} \right)}{\frac{V^2}{W^2} + 1} \right), \quad (1)$$

where η_c , W , and T_c are the characteristic viscosity of the melt layer (Pa s), characteristic velocity (m/s), and characteristic temperature ($^{\circ}\text{C}$), respectively. T_c and η_c appear in the equation for the temperature dependence of viscosity:

$\eta(T) = \eta_c \exp(-(T - T_m)/T_c)$. W is defined as $W = \sqrt{\frac{8T_c K}{\eta_c}}$, where K is the thermal

conductivity of the melt. Along the melt layer boundaries (or $z = 0.5w$), $T(z) = T_m$, and a relationship between the shear stress (τ_{ss}), the thickness of the melt layer (w), and the slip rate (V) is derived from Eq. 1 (15):

$$w = \frac{W\eta_c}{\tau_{ss}} \frac{a \tanh \left(\frac{V/W}{\sqrt{\frac{V^2}{W^2} + 1}} \right)}{\frac{V^2}{W^2} + 1} \quad (2)$$

If both w and τ_{ss} are measured in the experiments conducted at different values of V . The two unknowns (η_c and W) can be determined by solving a system of

two equations (Eq.2). The thicknesses of the two experimentally formed pseudotachylyte (PST) layers were measured at different locations (n =10 in each case) under an optical microscope. The variable w_{meas} is the average thickness of the experimental pseudotachylyte. At the end of each experiment, the slip was decelerated and then ceased. Because the melt layer thickness may change during the deceleration stage of slip, we added to w_{meas} the change in melt layer thickness during the slip deceleration (Δw), which is obtained from the measured axial displacement. Then, $w = w_{meas} + \Delta w$.

Sample ID	w_{meas} (m)	Δw (m)	w (m)
3694	0.319	0.071	0.390
3851	0.286	0.038	0.324

In Run #3694, where $V = 0.7$ m/s, $\tau_{ss} = 3.0$ MPa and $w_{ss} = 0.390$. In Run #3851, where $V = 0.2$ m/s, $\tau_{ss} = 4.7$ MPa and $w_{ss} = 0.324$. The values of η_c and W determined using the method described above are 13,920 Pa s and 0.169 m/s, respectively. $K = 1.6$ W/m/K for a temperature of 1400 °C (T_M) (20). As $W = \sqrt{\frac{8T_c K}{\eta_c}}$, for $\eta_c = 13920$ Pa s, $K = 1.6$ W/m/K and $T_c = 30.9$ °C; $W = 0.169$ m/s.

At $z = 0$ (or at the center of the melt layer), $T = T_M$. Thus, we obtain the following equation of V from Eq. 1:

$$V = W \sqrt{\left(\frac{1}{\exp((T_m - T_M)/T_c)} - 1 \right)}. \quad (3)$$

For $T_m = 1071$ °C, $T_c = 30.9$ °C, $W = 0.169$ m/s, and $T_M = 1400$ °C; $V = 34.7$ m/s.

Experimental data acquisition	Integration of field and experimental data
Rock friction tests on the wall rock ¹ at different slip rates (V) ² (Steady-state) shear stress (τ_{ss}) ³ Axial displacement during deceleration (change in melt layer thickness during deceleration) Measurement of slip zone temperature ⁴ Temperature raw data ⁵ Emissivity (ϵ) of slip zone materials (0.76-1.0) Observation of recovered specimens (Optical and electron microscopic observations) ⁶ Delineation of melt layer boundaries ⁷ Thickness of experimental PST (w): 3+6 ⁸ Estimation of clast fraction (ϕ) in experimental PST ⁹ Melting temperature (T at melt layer boundaries) (T_m): 4+5+6 ¹⁰ Maximum temperature in experimental PST (T_M): 4+5 ¹¹ Characteristic velocity (W): 1+2+7 ¹² Characteristic viscosity (η_c): 1+2+7 ¹³ Characteristic temperature (T_c) : 11+12+thermal conductivity (K) ¹⁴ Clastic fraction vs. T_M plot: 8+10	Observation of fault outcrop ¹⁵ Thickness (w) of natural PST ¹⁶ Relationship between PST and tuffisite Observation and analyses of wall rock and fault rock samples ¹⁷ Estimation of clast fraction (ϕ) in natural PST ¹⁸ Chemistry of PST and wall rock (XRF) ¹⁹ Maximum temperature in natural PST (T_M): 17+14 ²⁰ Slip rate (V) of natural fault: 9+13+19 ²¹ Viscosity of natural frictional melt (η): 18+19 ²² Relative viscosity of clast-bearing melt (η_{rel}): 17+21 ²³ Effective viscosity (η_{eff}): 21+22 ²⁴ Effective viscosity (η_{eff}) across PST layer : 9+19+21+22+23 ²⁵ Shear stress (τ_f): 15+20+24 ²⁶ Fault displacement (d) : material and thermal proerties +wall rock temperature (T_{wr}) +15+17+19+25

Figure DR1. Integration of field and experimental data. It shows the ways how the data were collected and analyzed in the study.

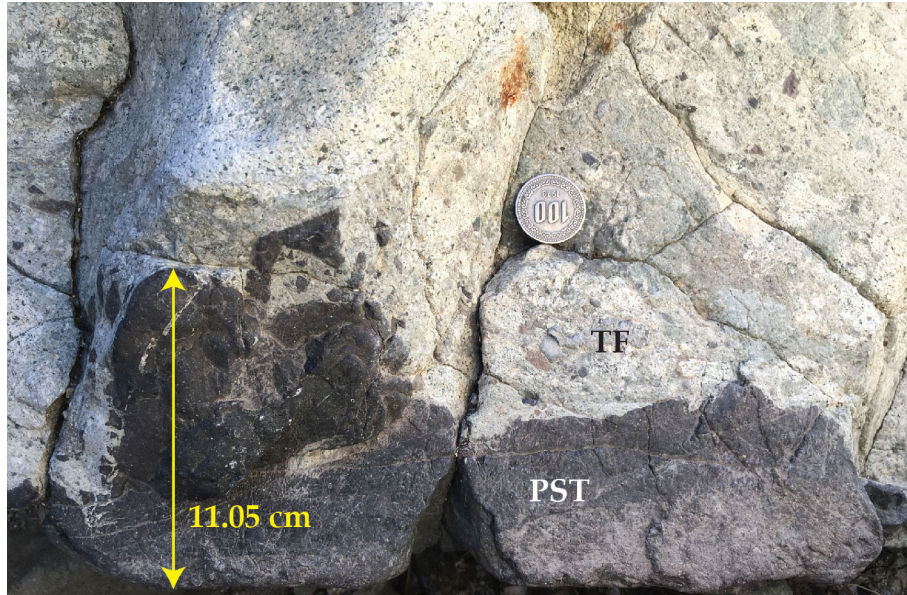


Figure DR2. The thickness of pseudotachylyte (PST) affected by tuffisite (TF) intrusion. A PST layer thicker than 10 cm is observed in some places but is mostly partially or fully detached from the main PST layer by tuffisite. Therefore, the original thickness of the PST could be greater than that observed.

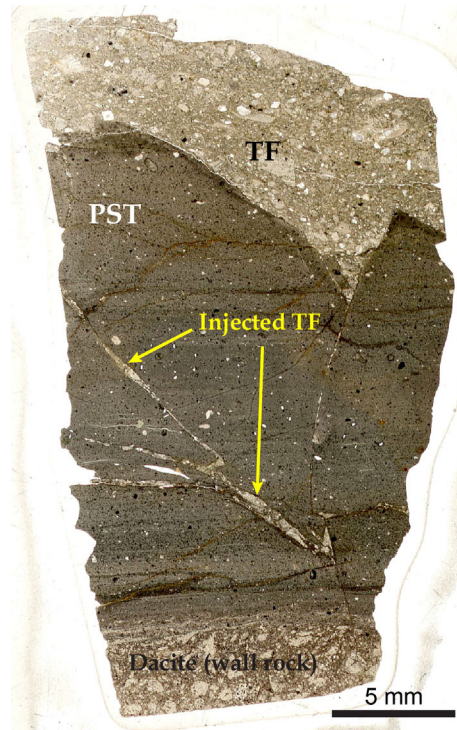


Figure DR3. Scanned thin-section image showing the tuffisite (TF) injected into the pseudotachylyte (PST) (plane-polarized light).

Table DR1. Clast fractions and maximum temperatures of the experimental melt layers.

Sample ID	Slip condition		Clast fraction, ϕ	Maximum temperature, T_M	
	Normal stress (MPa)	Slip rate (m/s)		$\varepsilon = 1.0$	$\varepsilon = 0.76$
3692	10	1.3	0.350	1072.5	1309.2
3694	10	0.7	0.342	1028.2	1253.6
3851	10	0.2	0.379	1016.6	1239.0
3931	5	1.3	0.307	1155.4	1413.4

Table DR2. Clast fraction determined by image analysis on natural PST.

Sample ID	Clast fraction, ϕ			
	Area 1	Area 2	Area 3	Average
SP-1V2	0.120	0.106	0.141	0.122
SP-3	0.144	0.066	0.257	0.156

Table DR3. Mineral composition of the wall rock determined by X-ray diffraction analysis.

	Volume fraction (%)
Quartz	25.9
Plagioclase	37.0
K-feldspar	12.4
Muscovite/illite	6.3
Biotite	3.0
Chlorite	5.1
Epidote	10.3
Total	100.0

Table DR4. Average chemical compositions (wt.%) of natural PST determined by X-ray fluorescence analysis.

	Natural PST (SJ-1)
SiO ₂	63.71
TiO ₂	0.70
Al ₂ O ₃	16.86
FeO	5.73
MnO	0.17
MgO	1.62
CaO	3.78
Na ₂ O	2.76
K ₂ O	2.74
P ₂ O ₅	0.16
F	-
H ₂ O	1.64*
Total	99.86

* Based on loss of ignition of XRF analysis.